Article

Not peer-reviewed version

Enhancing the Yield of Lab-on-a-Disk Based Single Image Parasite Quantification Device

Vyacheslav R Misko , Ramadhani Juma Makasali , Matthieu Briet , Filip Legein , Bruno Levecke , Wim De Malsche *

Posted Date: 30 September 2023

doi: 10.20944/preprints202309.2136.v1

Keywords: particle separation; parasite egg identification and quantification; diagnostic microfluidic device; extreme point-of-care

Article

Enhancing the Yield of Lab-on-a-Disk Based Single Image Parasite Quantification Device

Vyacheslav R. Misko [1], Ramadhani Juma Makasali [1], Matthieu Briet [1], Filip Legein [1], Bruno Levecke [2] and Wim De Malsche [1,*]

[1] μFlow group, Department of Bioengineering Sciences, Department of Chemical Engineering, Vrije Universiteit Brussel, Brussels, Belgium

[2] Department of Translational Physiology, Infectiology and Public Health, Ghent University, Merelbeke, Belgium

* Correspondence: Wim.De.Malsche@vub.be; Tel.: +32-2-6293781

Abstract: A recently proposed single image parasite quantification (SIMPAQ) platform based on a Lab-On-a-Disc (LOD) device has been earlier successfully tested in field conditions demonstrating the efficiency in soil-transmitted helminths (STH) egg detection and analysis. A related study (*Micromachines* 2021, **12**, 1032) revealed the effects that can limit the performance of a SIMPAQ method due to the action of the Euler and Coriolis forces, and the interaction of the moving eggs with the walls of the LOD chamber. Here we propose a new improved design that allows to overcome those limitations and enhance the yield of the SIMPAQ LOD device which is demonstrated in the experiments with synthetic particle model system and real parasite eggs.

Keywords: particle separation; parasite egg identification and quantification; diagnostic microfluidic device; extreme point-of-care

1. Introduction

A Lab-On-a-Disc (LOD) device was recently developed [1] for the detection of soil-transmitted helminths (STH), i.e., intestinal worms that infect humans and are spread through contaminated soil [2,3]. The LOD device is a centrifugal microfluidic platform based on centrifugation and flotation which isolates and collects eggs within an imaging zone using, e.g., saturated sodium chloride as flotation solution. The main advantage of this device as compared to other diagnostic methods (see, e.g., [4–8]) is that it holds promise to provide quick diagnostics where needed (point-of-care (POC) testing), requiring small amounts of sample and materials only. An image of a packed monolayer of eggs is collected within a single imaging zone, or field of view (FOV). A distinct feature of this system is that a parasite egg monolayer can be formed by restricting the chamber height of the imaging zone to the size of a single egg (as low as 60 μm). The platform was successfully tested in Ethiopia, Tanzania, Uganda and Kenya on infected human and animal samples for evaluation of the developed technology [9].

In turn, a LOD is a centrifugal microfluidic device that is a subclass of integrated Lab-on-a-Chip (LOC) platforms [10–13] that have advantages such as portability, the use of small amounts of materials and reagents, faster reaction times and time-to-result, programmability of process steps through varying the rotational conditions [11]. In addition to these, the LOD platform employs pseudo-forces generated during the rotation of the device: centrifugal force, the Coriolis force, and the angular acceleration-generated Euler force [12]. Several applications including clinical chemistry, immunoassay, cell analysis [14,15], and nucleic acid tests [16–18], have been demonstrated on a spinning disc [19]. Some applications of these LOD platforms are sample-to-answer systems for biomedical POC and global diagnostics [20], liquid handling automation for the life sciences, process analytical techniques and cell line development for biopharma as well as monitoring the environment, infrastructure, industrial processes and agrifood [21,22]. The LOD platform has been

Preprints (www.preprints.org) | NOT PEER-REVIEWED | Posted: 30 September 2023 doi:10.20944/preprints202309.2136.v1

applied for detection and molecular analysis of pathogens [23] such as, e.g., *Salmonella*, a major food-borne pathogen [24,25]. Recently, possibilities of employing LOD platforms for the detection of Covid-19 have been discussed in the literature as well [26].

The effect of the lateral walls of a LOD device on the dynamics of a model system of particles with a density lower than that of the solvent (modelling parasites eggs) has been analyzed theoretically and experimentally [27]. It has been shown that the trajectory of a particle moving under the action of the centrifugal force is deflected in the tangential direction by the inertial Coriolis and Euler forces, and that the particle easily reaches the lateral walls of the narrow channel. The walls, depending on the angle they form with the radial direction, can guide the particle either in the same or in the opposite direction to the centrifugal force, thus resulting in unusual particle trajectories including zig-zag or backwards particle motion [27] (see Figure 1b). This effect is pronounced in the case of short operation times and for repeated ramp up and down cycles when the acceleration of the angular rotation, and thus the Euler force, is considerable. This behavior has been observed in the experiment with particles of density lower than that of the solvent, i.e., modeling eggs.

The revealed unusual motion patterns represent undesirable effects that can prevent some parasite eggs from reaching the FOV of the LOD device and thus limiting its efficiency. Since the density of parasite eggs is lower than that of the solvent, they move towards the center of rotation during centrifugation. It is worth noting that the revealed behavior occurs mainly near the center of rotation where the centrifugal force is small, and the interplay of the tangential Euler and Coriolis forces and the interaction with the walls could cause the backward motion [27]. Therefore, the undesirable effects occur near the entrance to the FOV, as confirmed by the experimental observations. In addition, the channel has a smooth step near the entrance to the FOV [18,27] which can trap some eggs before they reach the FOV considering the strong decrease in the centrifugal force near the entrance to the FOV, as compared to its values in the rest of the channel.

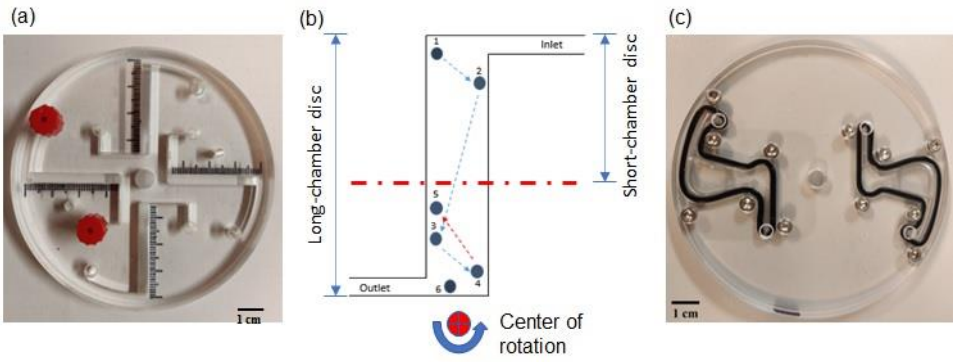

Figure 1. A long-chamber disc [27] (a). A typical trajectory of a particle (experiment) showing zig-zag and backwards motion near the center of rotation in a long-chamber disc [27]; the truncation of the chamber in a short-chamber disc is schematically shown by the dash-dotted red line (b). Short-chamber disc (c). .

One way to overcome this undesired effect, is to substantially increase the rotation speed of the disc which leads to very large tangential forces exerted on the eggs at the disc periphery that could be even damaging to the eggs (due to collision with the lateral walls). In addition, an excessive rotation speed increases the chance of a sudden leakage or disc precession. Thus, increasing the rotation speed is not an optimal solution. Alternatively, we propose to *reduce* the length of the channel (Figure 1), and in this way decrease the difference between the inertial forces, acting on the eggs, at the disc periphery and at the entrance to the FOV. In other words, we simply remove a part of the channel where the undesirable effects, i.e., a zig-zag and backwards motion, can occur. In this way, we expect that eggs reach the FOV at a reasonable operational rotation speed which enhances the yield of the LOD device. In this work, we perform experiments with synthetic particles modeling eggs and with real parasite eggs in a new LOD device with an improved design, and we compare the obtained results with those for the original ("long") disc [18,27].

 doi:10.20944/preprints202309.2136.v1

2. Experimental Setup & Materials

2.1. Imaging Set-Up

The imaging setup is shown in Figure 2. For capturing and storage of a single image for future examination, the Sony 1500 camera (FotoKonijnenberg, NL) was used throughout the experiments. The camera was connected to a Samyang Macro lens 2.8/100 mm (FotoKonijnenberg, NL). With the aid of an adaptor, the Macro lens was connected to an objective lens of 10× or 20× magnification power, depending on the experiments. To increase the visibility of the artificial parasite eggs (polystyrene particles) and the actual STHs eggs in the LOD, the imaging setup was connected to a halogen light source (Quartz Tungsten-Halogen lamp, Thorlabs).

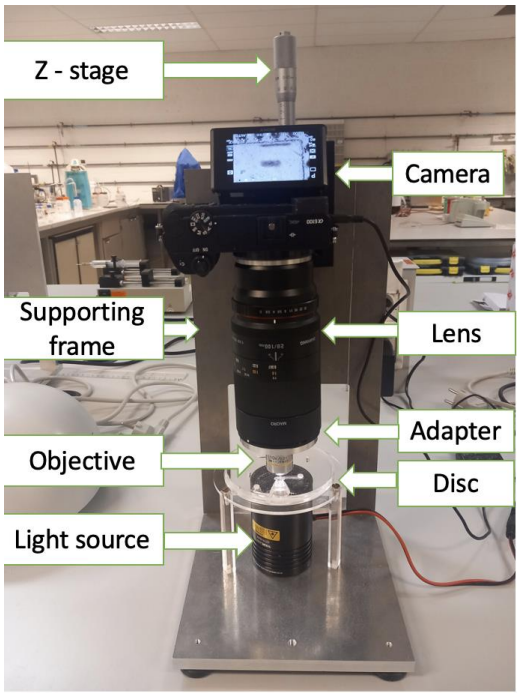

Figure 2. The imaging setup.

2.2. LOD Device: Short-Chamber vs. Long-Chamber Disc

The newly designed short-chamber LOD (Figure 3) produced from the plastic Poly (Methyl Methacrylate) (PMMA) possesses a shorter convergence chamber of 27 mm in length with a width and depth that decrease in size from the peripheral toward the rectangular section (collection zone/FOV). The chamber has a curved corner facing the sample entrance channel, whereas the length from the chamber to the center of the disc is 18 mm. The long-chamber LOD (Figure 3) is also produced from the plastic Poly (Methyl Methacrylate) (PMMA) and fabricated in a way that it possesses a longer convergence chamber of 37 mm length with a width and depth that decrease from the peripheral towards the rectangular section (collection zone/FOV). Also, the chamber has an angled corner opposite the sample entrance channel. The distance from the chamber to the center of the disc is 8 mm.

Preprints (www.preprints.org) | NOT PEER-REVIEWED | Posted: 30 September 2023 doi:10.20944/preprints202309.2136.v1

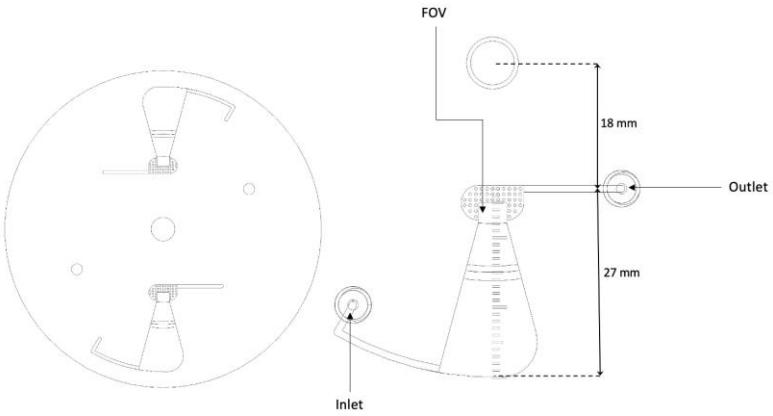

Figure 3. Computer-aided design (CAD) image of the short-chamber LOD with the indication of the total length of the chamber and the length from the chamber to the center of rotation.

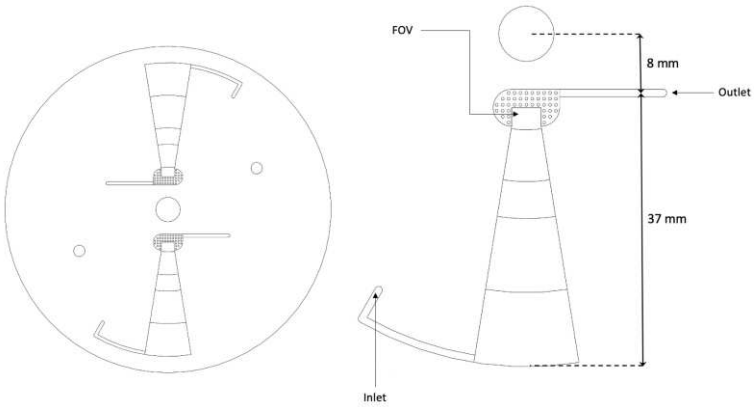

Figure 4. CAD image of the long-chamber LOD.

Figure 5 presents photographs of the modified reversible bound short-chamber LOD device, and a customized mini centrifuge (Eppendorf® Centrifuge MiniSpin G) [18,27] containing a reversibly bonded long-chamber LOD device.


(a)


(b)

Figure 5. (a) A photograph of the modified reversible bound short-chamber LOD device, and (b) a customized mini centrifuge containing a reversibly bonded long-chamber LOD device.

2.3. Flotation Solution for Particles and Eggs

 doi:10.20944/preprints202309.2136.v1

To prepare the flotation solution, 300 g of NaCl salt was measured on a weighing scale and dissolved in 1 liter of distilled water (Millipore Synergy UV, Spectralab Scientific lnc.). The magnetic stirrer together with the magnet rod was used to fasten the dissolution of the mixture until the NaCl salt was completely dissolved. Then, the density of the flotation solution was measured using the hydrometer and found to be 1.175 g/mL. The density of the flotation solution of 1.175 gmL^{-1} is higher than the densities of both the red polystyrene (PS) particles and STH eggs. The density of the red PS particles is 1.05 gmL^{-1}, the density of the *Ascaris* eggs is 1.11 g/mL, the density of hookworm eggs is 1.055 g/mL, and the density of the *Trichuris* eggs which are the heaviest among the STH eggs is 1.15 g/mL [28].

The experiments have been conducted with samples containing Ascaris eggs stored in ethanol, which can affect the density and migration behavior in the disc. The suspension also contains other particles and can also contain other parasites. In a follow-up study we will conduct the experiments directly after collection stool samples (avoiding storage in methanol) and will conduct a more detailed analysis on individual egg level and will explore for potential differentiation of the parasite species that are present.

3. Results and Discussion

3.1. The Influence of Chamber Design on the Trajectories of Polystyrene Particles

The experiment was conducted by initially introducing a single red PS particle in both the short-chamber LOD device and long-chamber LOD device, and centrifugation was performed at the rotation speed of 800 rpm (providing the acceleration of 15g, near the FOV, to 32g, at the periphery, where g = 9.81 m/s^2 is the acceleration due to gravity at the Earth surface), 1,000 rpm (23g to 50g), 1,500 (53g to 113g), and 2,000 rpm (94g to 201g) at a 5 s repeated centrifugation cycle until a PS particle reaches the FOV. The positions of the particles were recorded after each centrifugation cycle. For each rotation speed, the experiment was repeated 5 times.

At a rotation speed of 800 rpm two observations were made: (i) first, the time needed for PS particles to reach the FOV was appreciably longer than for higher rotation speed. Thus, in both the short-chamber and the long-chamber LOD, PS have varying x- and y-coordinate positions (see figure 6a and 6b) before they reach the FOV. In the short-chamber LOD device only 40% of PS particles (EXP 3 and EXP 5) reached the FOV in 10 s while the rest of the particles, 60% (EXP 1, EXP 2, and EXP 4), spent 15 s to migrate to the FOV (Figure 5a), while in the long-chamber LOD device, all PS particles, 100% (EXP 1, EXP 2, EXP 3, EXP 4 and EXP 5), spent 20 s to migrate to the FOV (Figure 6b). (ii) Second, for a rotation speed of 800 rpm in both LOD devices, the trajectories of the PS particles showed several zig-zag patterns (which are even more pronounced in rectangular chambers where backwards motions can also be observed, see Figure 1b) while migrating to the FOV (Figure 6a,b). These two observations result from the application of a relatively low rotation speed (800 rpm) that caused the generation of small relative centrifugal force (RCF), as discussed in [29]. Therefore, the generated small relative centrifugal force caused the denser flotation solution to move slowly to the periphery of the chamber and led to the generation of small buoyant force that caused the PS particles to move slowly to the FOV. During the motion, the inertial pseudo-forces, i.e., the Euler and the Coriolis forces, caused the sideway motion of the PS particles resulting in multiple zig-zag parts in the trajectories observed in both LOD devices. Similar trajectories with zig-zag parts of moving PS particles in the LOD device were observed in the recent study [27] where it was revealed that the magnitude of the rotation speed is one of the factors that can influence the direction of motion of a particle in a rotating disk, when the interplay of the Euler and Coriolis forces with the interaction of particles with the chamber walls can cause the particle to move either away or towards the center of rotation [27].

The relation between the magnitude of the rotation speed and the occurrence of zig-zag parts in the trajectories of the PS particles was also proven in the experiments when the rotation speed was increased. Thus, at a rotation speed of 1,000 rpm, zig-zag parts in the trajectories of the PS particles were much more pronounced in long-chamber disk LOD device than in short-chamber LOD device

Preprints (www.preprints.org) | NOT PEER-REVIEWED | Posted: 30 September 2023 doi:10.20944/preprints202309.2136.v1

(see Figure 6c,d). This observation is also supported in [29], where it is noted that the relative centrifugal force also depends on the distance of the particles from the center of rotation. Therefore, this could be the reason that there were fewer zig-zag parts in the trajectories of PS particles in the short-chamber LOD device, i.e., because the chamber is far from the center of rotation, and therefore the generated relative centrifugal force was somehow higher enough to generate the buoyant force that drove the PS particles to the FOV with less zig-zag patterns in the trajectories.

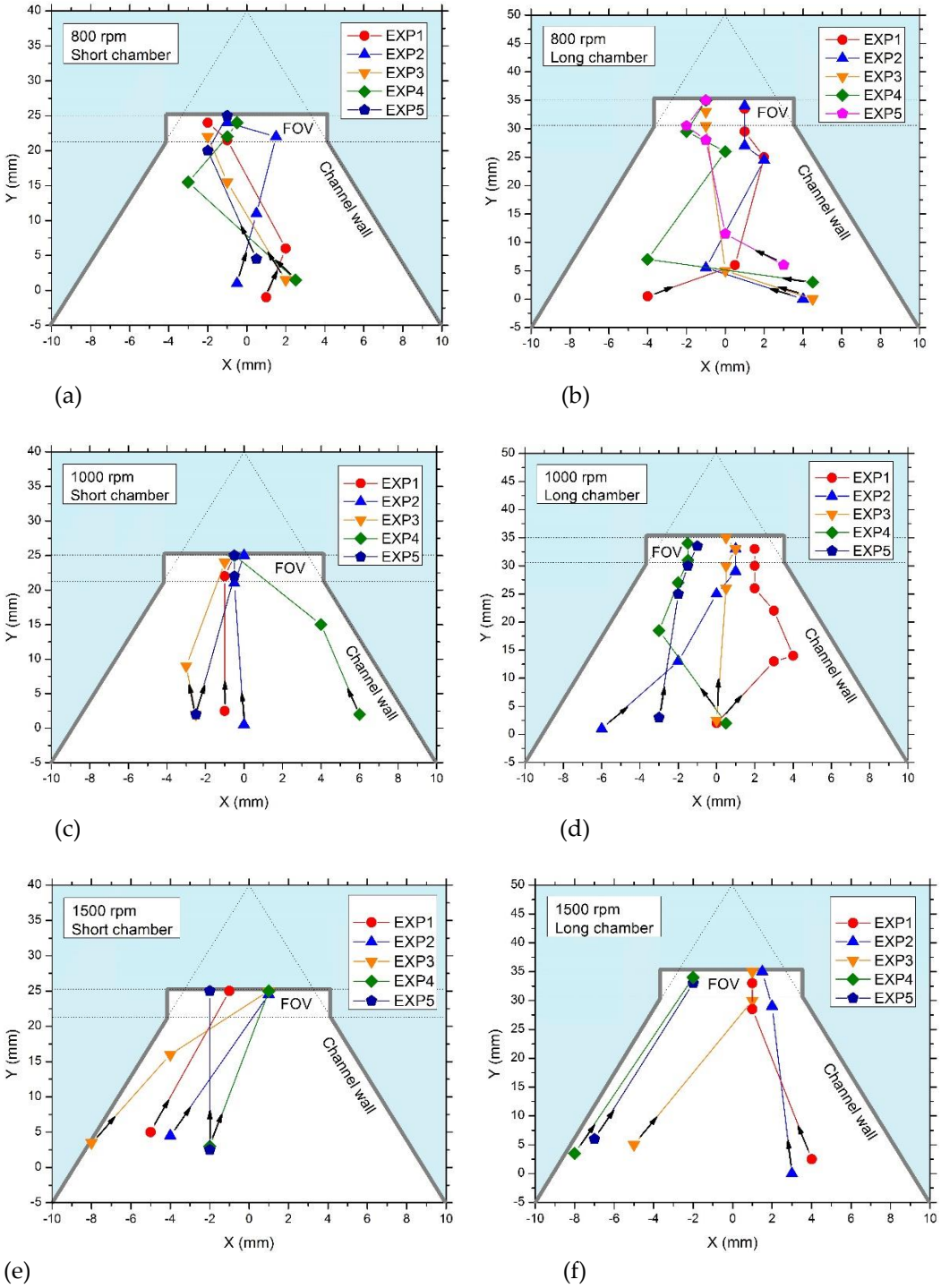

Figure 6. Trajectories of the red polystyrene particles in the short-chamber LOD and long-chamber LOD. (a), (c), (e), and (g): trajectories of five red polystyrene particles in short-chamber LODs. (b), (d), (f), and (h): trajectories of five red polystyrene particles in the long-chamber LODs. (a) and (b): the rotation speed is 800 rpm, (c) and (d): the rotation speed is 1,000 rpm, and (e) and (f): the rotation

speed is 1,500 rpm. For each rotation speed and each LOD device, there was a repeated cycle of 5 s centrifugation.

At a rotation speed of 1,500 rpm, 80% of the PS particles (EXP 1, EXP 2, EXP 4, and EXP 5) in the short-chamber LOD device (Figure 6e) reached the FOV without undergoing zig-zag parts in the trajectories whereas with the same rotation speed, in the long-chamber LOD device, only 40% (EXP 1 and EXP 2) managed to reach in the field FOV without undergoing zig-zag trajectories (Figure 5f). This result indicates that in the long-chamber LOD device, the Euler and Coriolis forces exerted on the particles are strong enough to cause the zig-zag patterns in the trajectories of the moving PS particles even when the rotation speed is 1,500 rpm (see Figure 6e,f).

Finally, at a rotation speed of 2,000 rpm, in both LOD devices, 100% of the PS particles managed to reach the FOV without undergoing zig-zag patterns in the trajectories. In addition, the time taken for the PS particles to reach the FOV was 5 s for all particles in both LOD devices (not shown).

The results of this experiment indicate that: (i) there is a relation between the magnitude of the rotation speed and the trajectories of the PS particles: it has been observed in the experiment that zig-zag parts in the trajectories of the particles decrease with the increase of the rotation speed, and (ii) this undesired effect is essentially suppressed in the short-chamber LOD, as compared to the long-chamber LOD.

3.2. Efficiency of the Short-Chamber LOD Device vs. Long-Chamber LOD Device in Delivering Polystyrene Particles to the FOV

To carry out this experiment, 100 red polystyrene particles were introduced in both the short-chamber LOD device and long-chamber LOD device, and the centrifugation was performed at the rotation speed of 1,000 rpm, 1,500 rpm, and 2,000 rpm for 1 min per each rotation speed. The experiment was repeated 3 times at each rotation speed.

The result of this experiment showed that, at the rotation speed of 1,000 rpm, 92.0±2.7% of the PS particles were delivered in the FOV in the short-chamber LOD device while the long-chambered LOD device showed a lower efficiency in delivering PS particles in the FOV, 82.7±3.2%. At a rotation speed of 1,500 rpm, the fraction of PS particles that reached the FOV in the short-chamber LOD device increased to 95.0±2.0% while for the long-chamber LOD device this fraction was 91±3.0% (Table 1). At a rotation speed of 2,000 rpm, the fraction of PS particles delivered to the FOV in short-chambered LOD device reached the value of 98.7±2.3%, where in 2 out of 3 experiments, the short-chamber LOD delivered 100% of the PS particles in the FOV. For the long-chamber LOD, the corresponding fraction of PS particles delivered in the FOV appeared to be 93.3±1.5% in 3 repeated experiments. These results indicate that the number of PS particles in the FOV increased with an increase in rotation speed in both LOD devices, and that the fraction of the particles delivered in the FOV is higher for the short-chamber LOD device.

So far, 2,000 rpm was the rotation speed with the highest yield in both short-chamber and long-chamber LOD devices. However, the short-chamber LOD device was superior to the long-chamber LOD, since it allowed delivering of 98.7±2.3% of the PS particles in the FOV.

In the long-chamber LOD device, generally, the PS particles which were not able to reach the FOV were often observed nearby the entrance of the FOV, which is indicative of an insufficient rotation speed used in this experiment (1,000 rpm, 1,500 rpm, and 2,000 rpm) for generating enough force for about 5% of PS particles to reach the FOV. This observation is in line with the conclusions of [30], claiming that the buoyant force increases when a cargo moves to pass a large depth. Therefore, when moving from the peripheral of the chamber towards the center of rotation of the LOD, the buoyant force that drives PS particles to reach the FOV decreases, and a higher rotation speed is needed to generate more force to compensate this decrease in the buoyant force. Furthermore, the many-particle effects such as their aggregation and interaction with the boundaries lead to further decrease of the driving force, which requires even a higher rotation speed to deliver PS particles in the FOV. In case of a single particle, the situation is different: at rotation speed of 2,000 rpm, the long-chamber LOD allowed to deliver single polystyrene red particles in the FOV in a very short time.

Preprints (www.preprints.org) | NOT PEER-REVIEWED | Posted: 30 September 2023 doi:10.20944/preprints202309.2136.v1

However, in the case of the short-chamber LOD device, the situation of many PS particles moving together to the FOV was not an issue because, as the results at the rotation speed of 2,000 rpm show, the short-chamber LOD device allowed to deliver 100% of the PS particles in the FOV in 2 out of 3 experiments, indicating that, since in the short chamber both the initial and the final points of the trajectory of moving PS particles are far from the center of rotation of the LOD, the rotation speed applied in this experiment was sufficient to generate enough buoyant force to deliver almost all polystyrene red particles (> 95%) to the FOV (see Figure 7). The results for the short-chamber and long-chamber discs and for the rotations peed of 1,000, 1,500 and 2,000 rpm are summarized in Figure 8.

Table 1. Proportion of red polystyrene particles in the FOV of short-chamber LOD device and long-chamber LOD device, for the rotation speed of 1000 rpm, 1500 rpm, and 2000 rpm.

LOD	Polystyrene red particles in the FOV (%)		
	1000 rpm	1500 rpm	2000 rpm
Short-chamber LOD device	92. 0 ±2.7%	95. 0 ±2.0%	98.7±2.3%
Long-chamber LOD device	82.7±3.2%	91.0±3.0%	93.3±1.5%

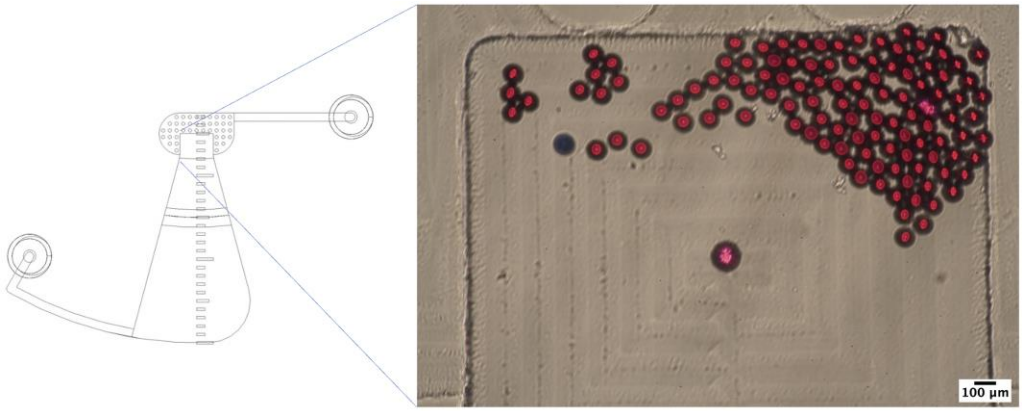

Figure 7. Red polystyrene particles in the FOV.

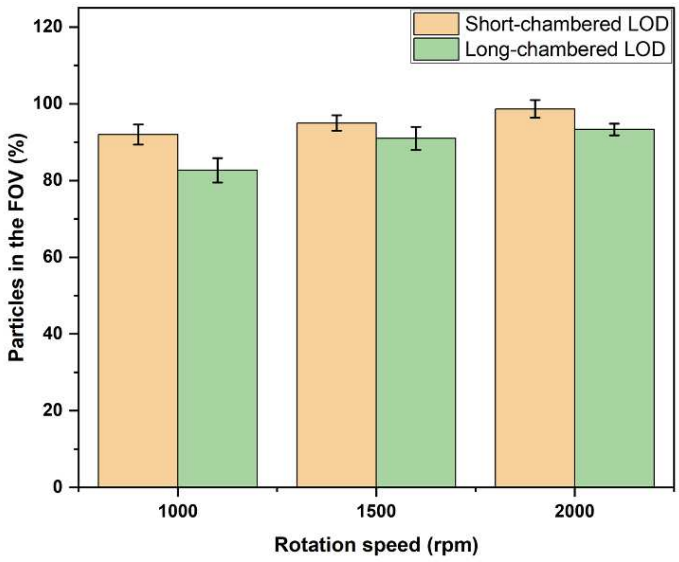

Figure 8. The average fraction of PS particles in the FOV versus rotation speeds in short-chamber and long-chamber LOD.

Preprints (www.preprints.org) | NOT PEER-REVIEWED | Posted: 30 September 2023 doi:10.20944/preprints202309.2136.v1

Therefore, these experiments demonstrated that the efficiency of the newly designed short-chamber LOD in delivering PS particles to the FOV is essentially higher than the corresponding efficiency of the long-chamber LOD device of the previous generation. Already at relatively moderate rotation speed of 2,000 rpm, which is also safe in terms of, e.g., potential leakage or precession (that can be observed at extremely high rotation speed), the new design, i.e., the short-chamber LOD, provides an excellent efficiency in delivering of PS particles in the FOV.

3.3. Efficiency of Short-Chamber and Long-Chamber LOD in Delivering STH Eggs in the FOV

The experiment was conducted by initially taking 100 µL of the stock sample containing purified eggs and mixed with 100 µL of distilled water. The mixture was centrifuged at the rotation speed of 1,500 rpm for 5 min. Following centrifugation, the supernatant was discarded, and the sediments were resuspended by adding 500 µL of the flotation solution of 1.175 g/mL density containing 0.05% Tween-20. Then, 500 µL of the suspension solution was loaded in chambers of short-chamber LOD device and long-chamber LOD device that were prefilled with the flotation solution of 1.175 g/mL density containing 0.05% Tween-20, and both devices were centrifuged at the rotation speed of 1,000 rpm (23g to 50g), 2,000 rpm (94g to 201g), 3,000 rpm (211g to 453g), and 4,000 rpm (376g to 805g) for 1 min at each rotation speed. The experiment was repeated 4 times for each rotation speed and LOD device.

The results of this experiment are in general in good agreement with those described above for PS particles indicating that the model system fairly reproduces the properties of real parasite eggs. As in the case of PS particles, the higher the rotation speed, the higher the fraction of the eggs delivered in the FOV. Also, short-chamber LOD device shows a higher efficiency in delivering eggs in the FOV as compared to the long-chamber LOD. The results for the short-chamber LOD vs. long-chamber LOD, for different rotation speed of 1,000 rpm, 2,000 rpm, 3,000 rpm, and 4,000 rpm are summarized in Table 2. Since we used the same flotation solution (density: 1.175 g/mL) for both the systems, PS particles (density: 1.05 g/mL) and STH eggs (density: 1.15 g/mL), the density contrast for STH eggs is lower than for PS particles which requires a higher rotation speed for achieving the same output, i.e., the fraction of the eggs delivered in the FOV. Therefore, the rotation speed was increased up to 4000 rpm in the experiments with STH eggs. The fraction of the STH eggs delivered in the FOV for the short-chamber and long-chamber LOD, for the rotation speed of 2000 rpm, 3000 rpm, and 4000 rpm, is shown in Figure 9, as an average (over four different experiments) fractions of the STH eggs delivered in the FOV for the short-chamber and long-chamber LOD. As shown in Figure 9, the fraction of the STH eggs delivered in the FOV gradually increases with the rotations speed for both the LOD devices from about 50% at 1,000 rpm to about 90% for the short-chambered LOD and about 80% for the short-chambered LOD, at 4,000 rpm. For all the rotation speed values, the efficiency in delivering STH eggs in the FOV for the short-chamber is superior to that for the long-chamber LOD device.

During conducting of this experiment, some of the STH eggs were blocked by fecal debris that have a low density comparable to the density of the STH eggs (see Figure 10) while migrating to the FOV in both short-chamber LOD device and long-chamber LOD device. Therefore, secondary purification of the stock sample to get a clear sample with STH eggs without much fecal debris was performed, as well as the experiment to investigate the efficiency of the short-chamber LOD device and the long-chamber LOD in delivering the real STH eggs to the FOV was conducted.

Table 2. Proportion of STH eggs in the FOV of short-chamber LOD device and long-chamber LOD device, for the rotation speed of 1000 rpm, 2000 rpm, 3000 rpm, and 4000 rpm.

LOD	STH eggs in the FOV (%)			
	1000 rpm	**2000 rpm**	**3000 rpm**	**4000 rpm**
Short-chamber LOD device	51.2±10.7%	67.2±7.3%	79.4±5.2%	89.8±2.6%
Long-chamber LOD device	48.7±10.3%	60.4±4.7%	73.0±4.7%	78.2±4.9%

Preprints (www.preprints.org) | NOT PEER-REVIEWED | Posted: 30 September 2023 doi:10.20944/preprints202309.2136.v1

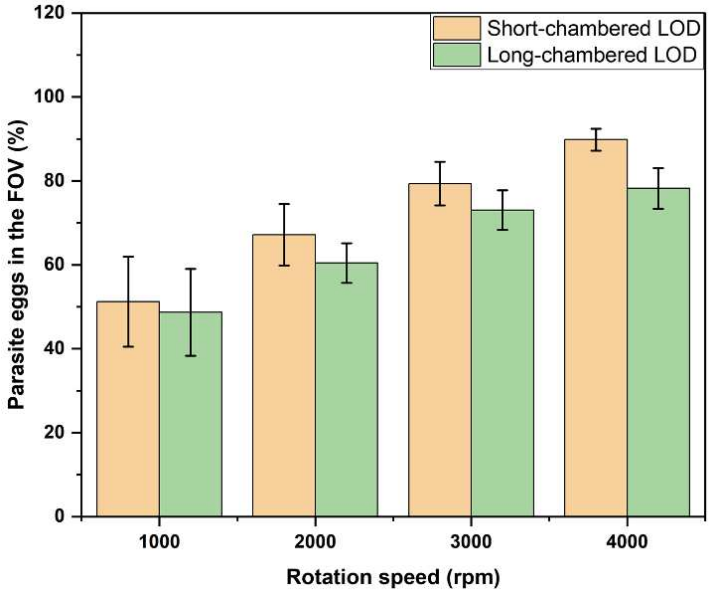

Figure 9. The average fraction of STH eggs in the FOV against rotation speeds in short-chamber LOD and long-chamber LOD.

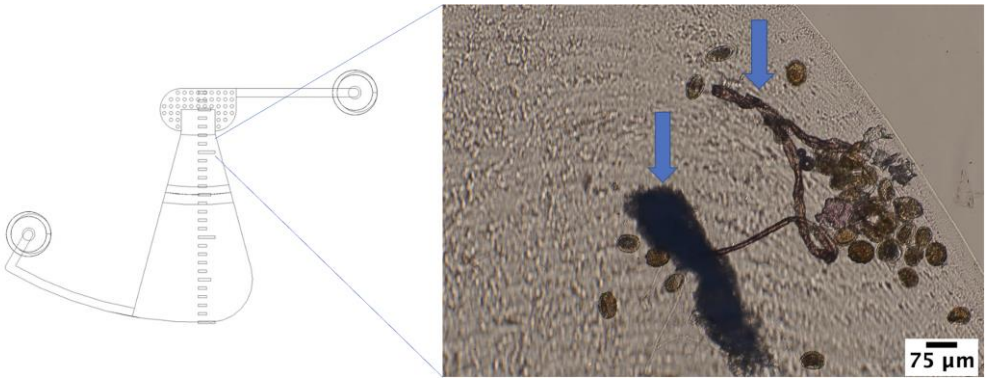

Figure 10. Some STH eggs got stuck on the way to the FOV due to fecal debris. Arrows indicate fecal debris.

4. Conclusions

The promise of the microfluidic Lab-On-a-Disc (LOD) device for the quantification and identification of STH eggs to diagnose STH infections has been recently shown. However, the developed LOD device with the chambers extended from the edge of the disk to the close vicinity of the center of rotation ("long-chamber" LOD device) has been confronted with a loss of some STH eggs in the FOV. Therefore, in this work, a new design of the disk with truncated chambers that end further away from the center of rotation ("short-chamber" LOD device) was developed, and its efficiency was compared with the long-chambered LOD device.

To achieve this goal, the influence of the chamber design on the trajectories of the red polystyrene (PS) particles (which serve as a model system for STH eggs) to the FOV was investigated. The zig-zag parts in the trajectories of the PS particles which always occur at lower rotation speeds were eliminated in both the long-chamber LOD device and short-chamber LOD device at 2,000 rpm rotation speed. However, at a rotation speed of 1,500 rpm, the short-chamber LOD device was able to deliver 80% of the PS particles to the FOV without zig-zag trajectory patterns, whereas the long-chamber LOD device was able to deliver only 40% of the PS particles to the FOV. This result indicates that even at 1500 rpm rotation speed the newly designed short-chamber LOD device can generate enough relative centrifugal force that can overcome to a large extent the effect of the Euler force and

Coriolis force that cause undesired distortions (like zig-zag and backward motion) of the trajectories of the PS particles.

The efficiency of the short-chamber LOD device and long-chamber LOD device in delivering PS particles in the FOV was investigated. The results revealed that at the rotation speed of 1,000 rpm, the short-chamber LOD device delivered 92.0±2.7% of the PS particles to the FOV whereas the long-chamber LOD device delivered 82.7±3.2% of the PS particles to the FOV. At the rotation speed of 1,500 rpm, the short-chamber LOD device delivered 95.0±2.0% of the PS particles to the FOV whereas the long-chamber LOD device 91.0±3.0%. At the rotation speed of 2,000 rpm, the short-chamber and long-chamber LOD devices delivered, correspondingly, 98.7±2.3% and 93.3±1.5% of the PS particles to the FOV. In both the short-chamber and the long-chamber LOD devices, the number PS particles increased with an increase in rotation speed. However, at each rotation speed used the short-chamber LOD device delivered more PS particles in the FOV than the long-chamber LOD device. This result also suggests that the newly designed short-chamber LOD device at each rotation speed produces more relative centrifugal force than the long-chamber LOD device, which leads to the generation of more buoyant force which drives more PS particles to the FOV.

We further investigated the efficiency of the short-chamber LOD device and long-chamber LOD device in delivering STH eggs in the FOV. The result obtained in this investigation is consistent with the result obtained when PS particles were used. Thus, the number of STH eggs in the FOV was increasing with the increase of the rotation speeds. Similar to the case of the PS particles, at each rotation speed used the short-chamber LOD device delivered more STH eggs in the FOV than the long-chamber LOD device. Therefore, the enhanced efficiency of the new designed short-chamber LOD device in delivering STH eggs to the FOV for the analysis has been demonstrated.

The sample preparation step using a 200 μm filter membrane and a 20 μm filter membrane improved the yield of STH eggs in the FOV of the LOD devices. However, fecal debris that managed to pass the 200 μm filter membrane was still observed to be an obstacle to some STH eggs in reaching the FOV. Based on the results obtained from this work it was found that the short-chamber LOD device has overcome to a large extent the problem that some STH eggs do not reach the FOV. Furthermore, to increase the sensitivity and to make the short-chamber LOD device more user-friendly in the field conditions, a 200 μm filter membrane and a 20 μm filter membrane can be incorporated into the chambers of the short-chamber LOD device so that the sample preparation step and the separation procedure can be integrated at the same time in the LOD technique.

We note that the experiments have been conducted with samples containing Ascaris eggs stored in ethanol, which can affect the density and migration behavior in the disc. The suspension can also contain other particles and parasites. In a further study we plan to conduct the experiments directly after collecting stool samples and will perform a more detailed analysis on individual egg level and explore for potential differentiation of the parasite species that are present.

Author Contributions: Conceptualization, V.R.M. and W.D.M.; methodology, V.R.M., F.L., B.L. and W.D.M.; formal analysis, R.J.M. and V.R.M.; investigation: experiment, R.J.M., with the input from V.R.M., M.B., B.L. and W.D.M.; resources, W.D.M.; writing—original draft preparation, V.R.M., and R.J.M., writing—review and editing, V.R.M., W.D.M. and B.L.; visualization, R.J.M. and M.B.; supervision, W.D.M. and V.R.M.; project administration, W.D.M. and F.L.; funding acquisition, W.D.M. All authors have read and agreed to the published version of the manuscript.

Funding: This research was funded by the Innovation counsel at VUB, grant number IOFPOC35 and by Vlir-Uos, grant number SI-2020-01-86 ('SIMPAQ in Tanzania').

Conflicts of Interest: The authors declare no conflict of interest.

References

1. S. Sukas, B. Van Dorst, A. Kryj, O. Lagatie, W. De Malsche, Development of a lab-on-a-disk platform with digital imaging for identification and counting of parasite eggs in human and animal stool, *Micromachines* **2019**, 10(12), 852.
2. WHO Newsletter, Soil-transmitted helminth infections, 2 March 2020.
3. Helminths, p.s.t., Centers for diseases and prevention. **2020**, p. 1.
4. R. L. Guerrant, Bench aids for the diagnosis of intestinal parasites-WHO, *Parasitology Today* **1995**, 6, 238.

5. B. Levecke, J. M. Behnke, S. S. R. Ajjampur, M. Albonico, S. M. Ame, J. Charlier, S. M. Geiger, N. T. V. Hoa, R. I. Kamwa Ngassam, A. C. Kotze, J. S. McCarthy, A. Montresor, M. V. Periago, S. Roy, L. -A. Tchuem Tchuenté, D.T.C. Thach, J. Vercruysse, A comparison of the sensitivity and fecal egg counts of the McMaster egg counting and Kato-Katz thick smear methods for soil-transmitted helminths, *PLoS Negl Trop Dis* **2011**, 5(6), e1201.
6. B. D. Barda, L. Rinaldi, D. Ianniello, H. Zepherine, F. Salvo, T. Sadutshang, G. Cringoli, M. Clementi, M. Albonico, Mini-FLOTAC, an innovative direct diagnostic technique for intestinal parasitic infections: experience from the field, *PLoS Negl Trop Dis* **2013**, 7(8), e2344.
7. L. Rinaldi, G.C. Coles, M.P. Maurelli, V. Musella, G. Cringoli, Calibration and diagnostic accuracy of simple flotation, McMaster and FLOTAC for parasite egg counts in sheep, *Veterinary Parasitology* **2011**, 177(3-4), 345-352.
8. W. Moser, O. Bärenbold, G.J. Mirams, P. Cools, J. Vlaminck, S.M. Ali, S.M. Ame, J. Hattendorf, P. Vounatsou, B. Levecke, J. Keiser, Diagnostic comparison between FECPAKG2 and the Kato-Katz method for analyzing soil-transmitted helminth eggs in stool, *PLoS Negl Trop Dis* **2018**, 12(6), e0006562.
9. S. L. Rubagumya, J. Nzalawahe, G. Misinzo, H. Mazigo, M. Briet, V. R. Misko, W. De Malsche, F. Legein, N. C. Justine, N. Basinda, M. Zinga, E. Mafie, Preliminary evaluation of Lab-On-a_Disc (LOD) technique for diagnosis of soli-transmitted helminths in animals, Morogono-Tanzania, Submitted to *Parasitology* (2003).
10. M. Madou, J. Zoval, G. G. Jia, H. Kido, J. Kim, and N. Kim, Lab on a CD, *Annu. Rev. Biomed. Eng.* **2006**, 8, 601–28.
11. S. Smith, D. Mager, A. Perebikovsky, E. Shamloo, D. Kinahan, R. Mishra, S. M. T. Delgado, H. Kido, S. Saha, J. Ducrée, M. Madou, K. Land and J. G. Korvink, CD-Based Microfluidics for Primary Care in Extreme Point-of-Care Settings, *Micromachines* **2016**, 7, 22.
12. L. X. Kong, A. Perebikovsky, J. Moebius, L. Kulinsky, and M. Madou, Lab-on-a-CD: A Fully Integrated Molecular Diagnostic System, *J. Lab. Automation* **2016**, 21(3) 323–355.
13. J. Ducrée, Secure Air Traffic Control at the Hub of Multiplexing on the Centrifugo-Pneumatic Lab-on-a-Disc Platform, *Micromachines* **2021**, 12, 700.
14. H. Kido, M. Micic, D. Smith, J. Zoval, J. Norton, M. Madou, A novel, compact disk-like centrifugal microfluidics system for cell lysis and sample homogenization, *Colloids and Surfaces B: Biointerfaces* **2007**, 58, 44–51.
15. A. K. Jahromi, M. Saadatmand, M. Eghbal and L. P. Yeganeh, Development of simple and efficient Lab-on-a-Disc platforms for automated chemical cell lysis, *Sci. Rep.* **2020**, 10, 11039.
16. E. Roy, G. Stewart, M. Mounier, L. Malic, R. Peytavi, L. Clime, M. Madou, M. Bossinot, M. G. Bergeronb and T. Veres, From cellular lysis to microarray detection, an integrated thermoplastic elastomer (TPE) point of care Lab on a Disc, *Lab. Chip.* **2015**, 15, 406.
17. H. V. Nguyen, V. D. Nguyen, H. Q. Nguyen, T. H. T. Chau, E. Y. Lee, T. S. Seo, Nucleic acid diagnostics on the total integrated lab-on-a-disc for point-of-care testing, *Biosensors and Bioelectronics* **2019**, 141, 111466.
18. D. King, M. D. Glynn, S. Cindric, D. Kernan, T. O'Connell, R. Hakimjavadi, S. Kearney, T. Ackermann, X. M. Berbel, A. Llobera, U. Simonsen, B. E. Laursen, E. M. Redmond, P. A. Cahill and J. Ducrée, Label-Free Multi parameter optical Interrogation of endothelial Activation in single Cells using a Lab on a Disc platform, *Sci. Rep.* **2019**, 9, 4157.
19. T. Kim, V. Sunkara, J. Park, C. Kim, H. Woo and Y. Cho, Lab-on-a-disc with reversible and thermally stable diaphragm valves, *Lab. Chip*. **2016**, 16, 3741-3749.
20. R. Gorkin, J. Park, J. Siegrist, M. Amasia, B. S. Lee, J.-M. Park, J. Kim, H. Kim, M. Madou and Y.-K. Cho, Centrifugal microfluidics for biomedical applications, *Lab. Chip.* **2010**, 10, 1758–1773.
21. J. Ducrée, Design Optimization of Centrifugal Microfluidic "Lab-on-a-Disc" Systems towards Fluidic Larger-Scale Integration, *Appl. Sci.* **2021**, 11, 5839.
22. N. A. Rahman, F. Ibrahim, M. M. Aeinehvand, R. Yusof and M. Madou, A Microfluidic Lab-on-a-Disc (LOD) for Antioxidant Activities of Plant Extracts, *Micromachines* **2018**, 9, 140.
23. A. Sayad, F. Ibrahim, S. M. Uddin, J. Cho, M. Madou, K. L. Thong, A microdevice for rapid, monoplex and colorimetric detection of foodborne pathogens using a centrifugal microfluidic platform, *Biosensors and Bioelectronics* **2018**, 100, 96–104.
24. T.-H. Kim, J. Park, C.-J. Kim, Y.-K. Cho, Fully integrated lab-on-a-disc for nucleic acid analysis of food-borne pathogens, *Anal Chem*. **2014**, 86(8), 3841-8.
25. A. A. Sayad, F. Ibrahim, S. M. Uddin, K. X. Pei, M. S. Mohktar, M. Madou, K. L. Thong, A microfluidic lab-on-a-disc integrated loop mediated isothermal amplification for foodborne pathogen detection, *Sensors and Actuators B* **2016**, 227, 600–609.
26. T. Ji, Z. Liu, G. Q. Wang, X. G. Guo, S. A. Khan, C. C. Lai, H. Chen, S. Huang, S. M. Xia, B. Chen, H. Y. Jia, Y. C. Chen, Q. Zhou, Detection of COVID-19: A review of the current literature and future perspectives, *Rev. Biosens. Bioelectron.* **2020**, 166, 112455.

27. V. R. Misko, A. Kryj, A.-M. T. Ngansop, S. Yazdani, M. Briet, N. Basinda, H. D. Mazigo, W. De Malsche, Migration Behavior of Low-Density Particles in Lab-on-a-Disc Devices: Effect of Walls, *Micromachines* 2021, **12**, 1032.
28. M. Ayana et al., Modification and optimization of the FECPAKG2 protocol for the detection and quantification of soil-transmitted helminth eggs in human stool, *PLoS Negl Trop Dis*, 2018, **12** (10), doi: 10.1371/journal.pntd.0006655.
29. S. O. Majekodunmi, A Review on Centrifugation in the Pharmaceutical Industry, *Am J Biomed Eng*, 2015, 5 (2), 67–78, doi: 10.5923/j.ajbe.20150502.03.
30. W. Wongsuwan and J. Huntula, The students' basic conceptions of buoyant force, *Journal of Physics: Conference Series*, Institute of Physics Publishing, 2019, doi: 10.1088/1742-6596/1380/1/012139.